

Thermally managed ring-cavity design enables LED-pumped Nd,Ce:YAG continuous wave single-longitudinal-mode laser for cost-effective precision photonics

Rong-Rong Jiang(江容容), Rui-Ze Xia(夏瑞泽), Feng-Yang Xing(邢凤阳), Liang Chen(陈亮), Yang Chen(陈阳), Feng-Bo Zhang(张峰博), Huan-Yu Zuo(左环宇), Jian-Ping Shen(沈建平), and Ling-Hai Xie(解令海)
Citation: Chin. Phys. B, 2026, 35 (**3**): 034203. DOI: 10.1088/1674-1056/adfbd5
http://cpb.iphy.ac.cn; http://iopscience.iop.org/cpb

What follows is a list of articles you may be interested in

Pulsed single-longitudinal-mode operation based on modal-gain difference in repetitively passively *Q*-switched lasers

Jinhe Yuan(袁晋鹤), Mofan Yang(杨莫凡), and Ziyi Wu(武子怡)
Chin. Phys. B, 2025, 34 (**7**): 074210. DOI: 10.1088/1674-1056/adc665

Single-frequency linearly polarized *Q*-switched fiber laser based on Nb_2GeTe_4 saturable absorber

Si-Yu Chen(陈思雨), Hai-Qin Deng(邓海芹), Wan-Ru Zhang(张万儒), Yong-Ping Dai(戴永平), Tao Wang(王涛), Qiang Yu(俞强), Can Li(李灿), Man Jiang(姜曼), Rong-Tao Su(粟荣涛), Jian Wu(吴坚), and Pu Zhou(周朴)
Chin. Phys. B, 2023, 32 (**7**): 074203. DOI: 10.1088/1674-1056/acad6d

Continuous-wave Nd:$KGd(WO_4)_2$ single-longitudinal-mode laser

Rui-Jun Lan(兰瑞君), Guang-Hua Liu(刘广华), Huan-Huan Min(闵欢欢), Tong-Yu Dai(戴通宇), Ying-Jie Shen(申英杰), Peng-Hua Mu(穆鹏华), Cheng Ren(任承), De-Zhong Cao(曹德忠), and Xavier Mateos
Chin. Phys. B, 2021, 30 (**8**): 084201. DOI: 10.1088/1674-1056/abea99

A single-longitudinal-mode continuous-wave Ho^{3+}: YVO_4 laser at 2.05 μm pumped by a Tm-fibre laser

Jing Wu(吴婧), Youlun Ju(鞠有伦), Zhenguo Zhang(张振国), Liwei Xu(徐丽伟), Tongyu Dai(戴通宇), Baoquan Yao(姚宝权), Yuezhu Wang(王月珠)
Chin. Phys. B, 2017, 26 (**1**): 014204. DOI: 10.1088/1674-1056/26/1/014204

Latest development of display technologies

Hong-Yue Gao(高洪跃), Qiu-Xiang Yao(姚秋香), Pan Liu(刘攀), Zhi-Qiang Zheng(郑志强), Ji-Cheng Liu(刘吉成), Hua-Dong Zheng(郑华东), Chao Zeng(曾超), Ying-Jie Yu(于瀛洁), Tao Sun(孙涛), Zhen-Xiang Zeng(曾震湘)
Chin. Phys. B, 2016, 25 (**9**): 094203. DOI: 10.1088/1674-1056/25/9/094203

Thermally managed ring-cavity design enables LED-pumped Nd,Ce:YAG continuous wave single-longitudinal-mode laser for cost-effective precision photonics

Rong-Rong Jiang(江容容)[1], Rui-Ze Xia(夏瑞泽)[1], Feng-Yang Xing(邢凤阳)[1], Liang Chen(陈亮)[1], Yang Chen(陈阳)[1], Feng-Bo Zhang(张峰博)[1], Huan-Yu Zuo(左环宇)[1], Jian-Ping Shen(沈建平)[1,†], and Ling-Hai Xie(解令海)[2]

[1] *College of Electronic and Optical Engineering & College of Flexible Electronics, Nanjing University of Posts and Telecommunications, Nanjing* 210023, *China*

[2] *State Key Laboratory of Organic Electronics and Information Displays & Institute of Advanced Materials (IAM), Nanjing University of Posts & Telecommunications, Nanjing* 210023, *China*

(Received 12 June 2025; revised manuscript received 27 July 2025; accepted manuscript online 15 August 2025)

We present a continuous wave (CW) single-longitudinal-mode (SLM) laser with a ring cavity based on efficient light-emitting diodes (LEDs)-pumped Nd,Ce:YAG dual-rod laser modules. In the free-running regime, a maximum average power of 4.27 W at 1064 nm is obtained, corresponding to the highest optical conversion efficiency of 5.1% and a slope efficiency of 13.9%. When operating in SLM configuration, the laser maintains a stable CW output of 200 mW with beam quality factors (M^2) measuring 1.44 and 1.30 along orthogonal *x*- and *y*-axes respectively. Spectral analysis reveals an emission linewidth of 70.76 MHz at maximum SLM output. This work represents, to the authors' knowledge, both the first successful implementation and the highest recorded performance characteristics for an LED-pumped Nd,Ce:YAG CW SLM laser system utilizing ring cavity configuration.

Keywords: single-longitudinal-mode, light-emitting diode, Nd,Ce:YAG, ring cavity

PACS: 42.55.–f, 42.55.Ye, 42.55.Xi, 42.60.Gd

DOI: 10.1088/1674-1056/adfbd5 **CSTR:** 32038.14.CPB.adfbd5

1. Introduction

All-solid-state CW SLM lasers demonstrate distinctive advantages including low noise, narrow linewidth, superior beam quality, and high operational stability, finding extensive applications in precision measurement, ultra-fine spectroscopy, quantum communication, lidar systems, laser remote sensing, and advanced material processing.[1–8] Numerous strategies have been developed to achieve SLM operation in all-solid-state lasers, including the use of FP etalon,[9,10] twisted-mode cavity,[11,12] short-cavity,[13,14] travelling-wave ring-cavity,[15,16] injection-seeding cavity.[17] Among these, the traveling-wave ring cavity is particularly advantageous for SLM generation, as it effectively mitigates spatial hole-burning effects and supports stable unidirectional oscillation through the incorporation of optical isolators.

While laser diodes (LDs) have traditionally dominated as pumping sources for single-longitudinal-mode (SLM) lasers.[18] Recent studies, however, have demonstrated that high-power LEDs can effectively serve as alternative pump sources for generating stabilized SLM lasers.[19–23] Compared to LD systems, LEDs exhibit broader emission spectra that enhance spectral overlap with the gain medium's absorption lines, thereby improving energy transfer efficiency. Furthermore, advancements in LED technology have significantly increased the optical power of single LED chip to the watt level, while by an order of magnitude over the past decade, enabling large-scale commercial applications of LEDs as pump sources.[24,25] However, due to the Lambertian emission characteristics of LEDs, their pumping efficiencies remain lower than that of LDs. Additionally, high-power LED arrays operated in CW mode require careful consideration of thermal constraints and application-specific requirements. These factors underscore the critical need for further exploration into LED-pumped CW SLM lasers, especially in light of their potential to provide a cost-effective, stable, and compact alternative to conventional LD-based systems. In particular, the integration of ring-cavity configurations with LED pumping provides a promising path toward unidirectional oscillation and narrow-linewidth operation, which are essential for high-precision optical applications. Despite this promise, current literature on such systems remains limited, especially for lasers operating directly at 1064 nm using efficient ring-cavity designs. In this context, this work aims to demonstrate the feasibility and performance of a novel LED-pumped CW SLM laser system, thereby contributing to the development of cost-efficient and high-stability laser sources suitable for emerging photonic

[†]Corresponding author. E-mail: jianpingshen@njupt.edu.cn

© 2026 Chinese Physical Society and IOP Publishing Ltd. All rights, including for text and data mining, AI training, and similar technologies, are reserved.

technologies such as quantum metrology, precision navigation, and portable spectroscopy.

In this study, we address several critical challenges associated with an LED-pumped Nd,Ce:YAG CW SLM laser system through three principal innovations. First, a pentagonal LED array configuration surrounding the laser rod achieves sufficient pump density while necessitating enhanced heat dissipation capabilities. Second, an LED-side-pumped dual-rod Nd,Ce:YAG laser structure is developed to lower the laser oscillation threshold and enhance the pump power density within the cavity. Third, systematic optimization of ring resonator parameters enables high average power and conversion efficiency in free-running operation for LED-pumped ring-cavity lasers. Additionally, the design incorporates a polarizer to establish linear intracavity polarization and a Faraday isolator assembly (comprising a TGG crystal, high-strength magnet, and half-wave plate) to suppress counter-propagating waves and ensure unidirectional CW SLM operation. In the end, under the free-running operation, the laser system achieves a maximum CW average output power of 4.27 W at 1064 nm, with an optical conversion efficiency of 5.1% and a slope efficiency of 13.9%. Moreover, in the SLM operation, the laser system produces a maximum CW average output power of 200 mW with M^2 values of 1.44 and 1.30 along the x and y axes, respectively, accompanied by a spectral linewidth of 70.76 MHz.

2. Experimental setup

Figure 1(a) presents the experimental configuration of the CW SLM laser system, featuring two LED side-pumping modules integrated into a ring cavity. An Nd,Ce:YAG laser rod (Dong Jun Crystal; 5-mm diameter × 120-mm length; Nd^{3+}: 1.0 at.%, Ce^{3+}: 0.05 at.%–0.1 at.%) undergoes active cooling through 18 °C circulating water. Polished crystal surfaces with controlled roughness ensure uniform pump light distribution, while end-faces employ 1064-nm anti-reflection coatings for enhanced transmission efficiency. Each LED array consists of 20 LED beads (SST-10-IRD, 810 nm, 90° lens angle) arranged in five rows, forming a side-pumping source uniformly surrounding the laser rod as shown in Fig. 1(b). This geometry optimizes pump uniformity while mitigating thermal gradients in the gain medium. Thermal management employs water-cooled copper blocks maintained at 3 °C to stabilize LED operation. The figure-eight ring resonator (1970-mm optical path length) incorporates two plane-concave mirrors (M3/M4: 300-mm curvature radius) and two planar mirrors (M1/M2). High-reflectivity coatings (1028 nm–1080 nm) on M2–M4 contrast with M1's output coupler characteristics (1.5% and 3% transmittance at 1064 nm). Precision mirror alignment ensures optimal beam quality. Unidirectional operation is enforced through a composite optical isolator containing a Faraday rotator, half-wave plate, and Brewster-angle polarizer. This configuration effectively suppresses spatial hole-burning effects in the isotropic laser crystal, enabling stable CW SLM operation despite competing longitudinal modes.

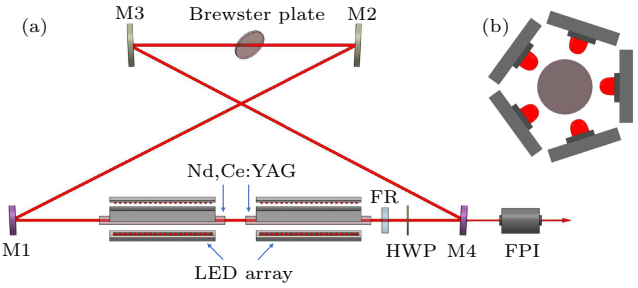


Fig. 1. (a) Schematic diagram of the CW SLM laser setup and (b) cross-sectional schematic diagram of fivefold symmetric LED pump module.

3. Results and discussion

Figure 2(a) presents comparative measurements of average output power for the 1064-nm laser in free-running operation under two distinct output coupling transmittances. With a $T = 1.5\%$ output coupler, the system achieves a maximum average output power of 4.27 W, corresponding to 5.1% optical conversion efficiency and 13.9% slope efficiency. In contrast, the $T = 3\%$ configuration yields reduced performance with 2.15-W maximum output power, 2.5% conversion efficiency, and 10.8% slope efficiency. Notably, neither configuration exhibits output power saturation, suggesting potential efficiency improvements through optimized pump power delivery and thermal management. Experimental data confirm superior performance metrics for the $T = 1.5\%$ mirror, demonstrating both lower lasing threshold and higher power output, thus establishing its selection for subsequent CW SLM experiments. Figure 2(b) details SLM operational characteristics, revealing a maximum CW output power of 200 mW ($T = 1.5\%$) with 1.2% slope efficiency. The substantial efficiency reduction compared to free-running operation arises primarily from intracavity losses induced by the Brewster polarizer, mirror interfaces, and diffraction effects. To the authors' knowledge, this work constitutes the first successful implementation of an LED-pumped Nd,Ce:YAG CW SLM laser in ring cavity configuration while simultaneously achieving record performance parameters for this laser architecture.

Figure 3 inset displays normalized spectral characteristics of the LED-pumped Nd,Ce:YAG CW laser in ring cavity configuration across both operational modes. Spectral measurements conducted using an Ocean Optics HR4000 spectrometer (resolution: 0.02 nm) reveal identical peak wavelengths of 1063.68 nm under free-running and SLM conditions, both exhibiting matching full width at half maximum (FWHM) values of 1.10 nm. This spectral consistency between operational regimes confirms wavelength stability during mode transition while maintaining equivalent linewidth characteristics.

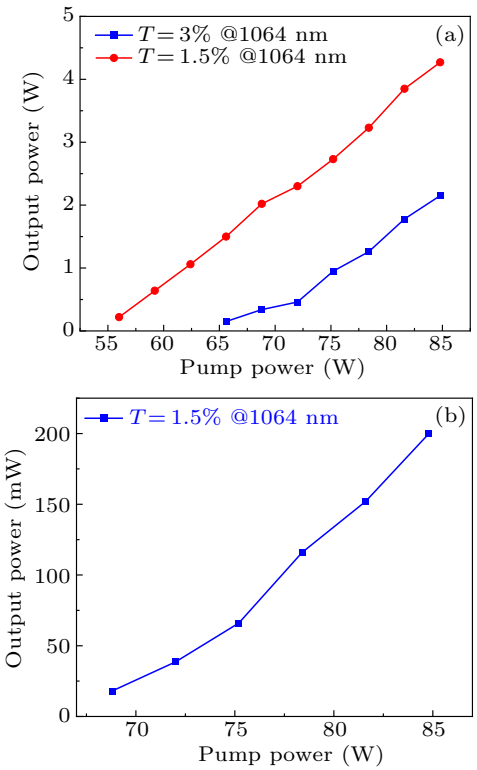


Fig. 2. The 1064-nm average output power *versus* LED incident power in (a) the free-running operation and (b) the SLM operation.

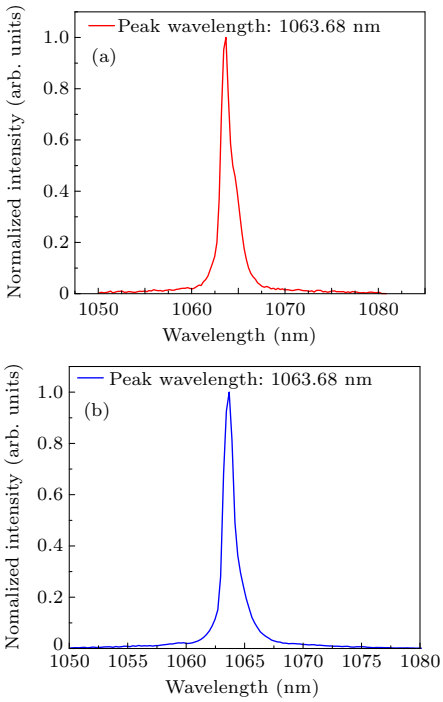


Fig. 3. The spectrum of (a) the free-running laser and (b) the SLM laser.

Figure 4 characterizes longitudinal mode behavior of the free-running CW laser through measurements employing a Fabry–Perot interferometer (FPI 801-1064, 2.5-GHz free spectral range). After passing through the FPI, the laser signal is detected by a fast photodiode (Thorlabs PDA10A2) connected to a digital oscilloscope (Tektronix MDO3034). The FPI spectrum at maximum output power reveals two distinct traces: the blue waveform corresponds to the FPI controller's driving voltage, while the yellow trace displays longitudinal mode signatures. Analysis demonstrates primary multi-longitudinal-mode operation with pronounced mode competition, as evidenced by multiple oscillating peaks. This spectral behavior underscores the inherent challenges in attaining stable SLM operation without dedicated mode selection components.



Fig. 4. FPI longitudinal mode spectrum of the free-running CW laser.

Figure 5 characterizes operational features of the CW SLM laser. Initially, figure 5(a) displays the FPI spectrum at maximum output power. During the FPI scanning process, nonlinear response times of the piezoelectric ceramic during its reset phase may introduce measurement artifacts in photodetector signals. To address this limitation, only data from the rising edge of the FPI scanning sawtooth wave is considered for analysis. As shown in the scanning FPI spectrum, no higher-order transverse modes are observed, confirming that the CW laser operates in an SLM regime. Furthermore, figure 5(b) quantifies the temporal profile of a single FPI longitudinal mode spectrum of the CW SLM laser. And the laser's linewidth can be calculated using the following formulas:

$$\Delta\nu = \frac{\nu_{\mathrm{FPI}}}{\tau}\cdot\tau_{\mathrm{p}}, \tag{1}$$

$$\Delta\lambda = \frac{\Delta\nu\cdot\lambda^2}{c} = \frac{\nu_{\mathrm{FPI}}\cdot\tau_{\mathrm{p}}\cdot\lambda^2}{\tau\cdot c}, \tag{2}$$

where τ and τ_{p} represent the pulse period and individual pulse width displayed on the oscilloscope, respectively, $\lambda = 1063.68$ nm and a free spectral range $\nu_{\mathrm{FPI}} = 2.5$ GHz between two pulse peaks. To minimize measurement errors, the pulse period between two pulse peaks is measured at each rising edge and averaged. Similarly, the pulse width of a single FPI longitudinal mode spectrum at each rising edge is measured and averaged. After calculating $\tau = 14.75$ ms and $\tau_{\mathrm{p}} = 417.5$ μs. These derived averages are subsequently applied to Eqs. (1) and (2) for precise linewidth calculation. The computed spectral linewidth resolves to $\Delta\nu \approx 70.76$ MHz, corresponding to a wavelength variation $\Delta\lambda \approx 0.267$ pm. These quantitative results provide definitive confirmation of stable SLM operation in the CW laser system. Notably, the spectrometer-measured FWHM exceeds the FPI-derived

linewidth by approximately two orders of magnitude. And this discrepancy arises fundamentally from the Ocean Optics HR4000 spectrometer's inherent resolution limit, which proves insufficient to resolve the narrow linewidth achieved through FPI-based measurements. Ultimately, the comparative analysis underscores the superior resolution capabilities of the FPI technique for precise spectral characterization of SLM lasers.

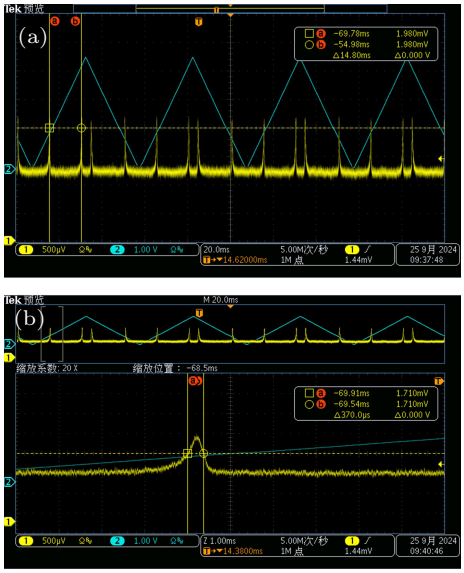


Fig. 5. (a) FPI longitudinal mode spectrum of the SLM laser. (b) Individual FPI longitudinal mode spectra of the SLM laser.

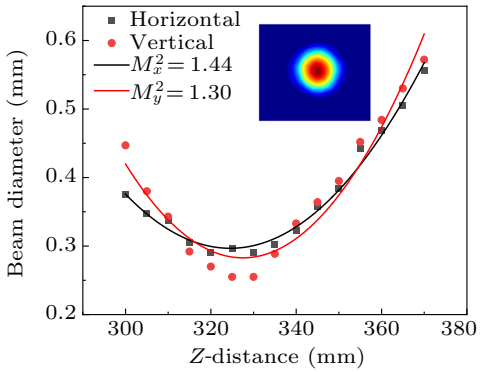


Fig. 6. Beam quality and two-dimensional laser beam profiles of the CW SLM laser.

Figure 6 shows the spatial beam profile near the laser beam waist for the CW SLM laser under moderate output power conditions. The beam profiles of the SLM laser are recorded at multiple positions using a beam analyzer (Cinogy CMOS-1201). Through least-squares fitting, the M^2 factors are determined to be 1.44 and 1.30 in the x-and y-directions, respectively. The inset in Fig. 6 presents the far-field beam profile captured by a CCD camera, confirming that the CW SLM laser operates in the TEM_{00} mode. At elevated pump powers, notable thermal effects are observed in the laser crystal, including increased thermal lensing, which alters the internal focusing conditions of the resonator. In the dual-rod configuration, both crystals contribute to an effective thermal lens, leading to cumulative focusing and enhanced sensitivity to thermal variations.[26]

This results in pronounced fluctuations in the spot radius at the crystal position, characterized by a reduced radial spot radius and increased fluctuation amplitude. While the curved vector spot radius remains less affected, overall fluctuations intensify. These thermal effects disrupt cavity mode matching and compromise resonator single-frequency stability. To achieve high-power output and maintain stability in the ring cavity laser, further optimization of crystal cooling or pump power becomes essential to mitigate the thermal lens effect and reduce spot radius fluctuations.

Figure 7 examines the temporal stability of the SLM laser output by monitoring power fluctuations at 30-second intervals. After an initial power decrease during the first 2 minutes of operation, periodic oscillations emerge, attributable to thermal fluctuations in the active cooling system. Over a 20-minute observation window, the root mean square (RMS) power variation remains below 1.6%, demonstrating exceptional long-term stability. This result aligns with the system's robust thermal management design and validates its operational reliability for precision applications requiring consistent SLM performance.

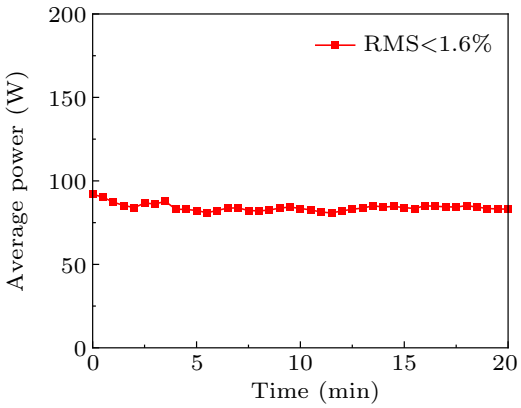


Fig. 7. Power fluctuations of the SLM laser over a twenty-minute period.

4. Conclusion

In conclusion, this study demonstrates successful achievement of stable SLM operation in an LED-pumped Nd,Ce:YAG CW laser employing a ring cavity configuration. The investigation establishes a notable technological advancement in infrared all-solid-state single-frequency laser development. While conventional SLM lasers predominantly utilize LD pumping architectures, this work establishes high-power LEDs as viable alternative pumping sources for generating stabilized SLM output. The system achieves a maximum free-running output of 4.27 W at 1064 nm with 5.1% optical conversion efficiency and 13.9% slope efficiency. In SLM operation, the laser delivers 200-mW CW output power, demonstrating beam quality factors of $M^2 = 1.44$ (x-axis) and

$M^2 = 1.30$ (y-axis) respectively, with a spectral linewidth measuring 70.76 MHz. To the authors' knowledge, this represents both the first experimental realization and the highest reported performance metrics for an LED-pumped Nd,Ce:YAG CW SLM laser in ring cavity configuration. These achievements validate the effectiveness of ring cavity designs in LED-pumped neodymium-doped crystal lasers for stable SLM generation. The research provides fundamental insights into LED-based pumping methodologies for solid-state lasers, establishing critical groundwork for future development and practical implementation of this technology across precision optical applications.

Acknowledgements

Project supported by the Fund from Nanjing University of Posts and Telecommunications, China (Grant Nos. KH1060325073, POCC2025M05, and NY225119) and the Key Research and Research and Development Program of Shandong Province, China (Grant No. 2021CXGC010202).

References

[1] Li J, Su H Y, Zhao C M, Zhang H Y and Xie W 2011 *Appl. Opt.* **50** 1329
[2] Dai T Y, Guo S X, Duan X M, Dou R Q and Zhang Q L 2019 *Phys. Opt. Express* **27** 34204
[3] Dai T Y, Ju Y L, Yao B Q, Shen Y J, Wang W and Wang Y Z 2012 *Opt. Lett.* **37** 1850
[4] Dai T Y, Ju Y L, Duan X M, Liu W, Yao B Q and Wang Y Z 2023 *Appl. Phys. B: Lasers Opt.* **111** 89
[5] Ma Y J, Li W, Wu H H, Chen W M, Wang Y L and Gu S J 2008 *Opt. Express* **16** 18702
[6] Yang X Z, Kitzler O, Spence D J, Bai Z X, Yan F and Mildren R P 2017 *Opt. Lett.* **45** 1898
[7] Wang K X, Gao C C, Lin Z F, Wang Q, Gao M W, Huang S and Chen C C 2020 *Opt. Express* **28** 14694
[8] Chen S Y, Deng H Q, Zhang W R, Zhang W R, Dai Y P, Wang T, Yu Q, Li C, Jiang M, Su R T and Wu J 2023 *Chin. Phys. B* **32** 074203
[9] Song B A, Zhao W J, Ren D M, Qu Y C, Zhang H Y, Qian L M and Hu X Y 2009 *Chin. Opt. Lett.* **7** 805
[10] Yao B Q, Chen F, Zhang C H, Wang Q, Wu C T and Duan X M 2011 *Opt. Lett.* **36** 1554
[11] Dai T Y, Wang Y P, Guo S X, Ju Y L, Duan X M and Yao B Q 2020 *Opt. Express* **28** 31775
[12] Cong Z H, Liu Z J, Qin Z G, Zhang X Y, Wang S W, Rao H and Fu Q 2015 *Appl. Opt.* **54** 5143
[13] Chen Y F, Bai Z X, Jin D, Li Y D, Qi Y Y, Ding J, Yan B Z, Wang K, Wang Y L and Lu Z W 2023 *Results Phys.* **46** 2211
[14] Lin Z, Gao C, Gao M and Weber H 2009 *Appl. Phys. B* **94** 81
[15] Shen D Y, Clarkson W A, Cooper L J and Williams R B 2004 *Opt. Lett.* **29** 2396
[16] Wu J, Ju Y L, Dai T Y, Yao B Q and Wang Y Z 2017 *Opt. Express.* **25** 27671
[17] Marienko I G, Zhi M, Khizhnyak A I and Sokolov A V 2020 *Opt. Express* **28** 25444
[18] Lu H D, Su J, Zheng Y H and Peng K C 2014 *Opt. Lett.* **39** 1117
[19] Shen J P, Xu S C, Lu P, Jiang R R, Wang W, Zhang S W, Xing F Y, Chen Y and Chen L 2024 *Chin. Phys. Lett.* **41** 034201
[20] Villars B, Hill E S and Durfee C G 2015 *Opt. Lett.* **40** 3049
[21] Shen J P, Lu P, Xu S C, Jiang R R, Chen L, Xing F Y and Chen Y 2024 *Appl. Phys. B* **33** 074207
[22] Zhao X B, Gustafsson A and Samuelson L 2023 *Chin. Phys. B* **32** 018103
[23] Cao Y W, Lv Q J, Yang T P, Mi T T, Wang X W, Liu W and Liu J L 2023 *Chin. Phys. B* **32** 058503
[24] Nourry-Martin M, Fermon N, Blanc C, Meignien L, Audebert P, Druon F, Georges P and Balembois F 2025 *Optica* **12** 3311
[25] Shen J P, Huang X, Xu S C, Lu P, Jiang S T and Jang R R 2023 *IEEE Photon. Technol. Lett.* **35** 721
[26] Shen J P, Lu P, Xu S C, Jiang R R, Chen Y, Chen L and Xing F Y 2024 *Chin. Phys. B* **33** 074207